EXPERIMENTAL CELL RESEARCH **236,** 66–75 (1997)
ARTICLE NO. EX973703

Effects of Intermittent or Continuous Gravitational Stresses on Cell–Matrix Adhesion: Quantitative Analysis of Focal Contacts in Osteoblastic ROS 17/2.8 Cells

Alain Guignandon,*[,1] Yves Usson,† Norbert Laroche,* Marie-Hélène Lafage-Proust,* Odile Sabido,‡ Christian Alexandre,* and Laurence Vico*

**Laboratoire de Biologie du Tissu Osseux, ‡Centre Commun de Cytométrie de Flux, Jean Monnet University, Saint-Etienne, France; and †Institut Albert Bonniot, Joseph Fourier University, Grenoble, France*

The relationship between cell morphology and cell metabolism and the role of mechanical load in bone remodeling is well known. Mechanical stimulation induces changes in the shape of osteoblasts, probably mediated by reorganization of focal contacts. We studied the influence of gravity (Gz) variations occurring during parabolic flight on osteoblast focal adhesion of ROS 17/2.8 osteosarcoma cells subjected to 15 or 30 parabolic flights. Significant flight-induced shape changes consisted of decreased cell area associated with focal contact plaque reorganization. Identical durations of continuous mechanical stress induced by centrifugation (2 Gz) or clinorotation (Gz randomization) had no major effect on cell focal adhesion. ROS 17/2.8 G2/M synchronization by treatment with nocodazole inhibited the flight-induced decrease in adhesion parameters. We concluded that ROS 17/2.8 cells are sensitive to Gz switches and that their adaptation is at least dependent on microtubule function. © 1997 Academic Press

INTRODUCTION

Bone matrix synthesis and mineralization of bone by osteoblasts are regulated by mechanical stimulation [1]. It is now well documented *in vivo* that an increase in mechanical stimulation increases osteoblast activities and bone mass. In contrast, microgravity decreases osteoblastic bone formation, leading to decreased bone mass and probably alteration of trabecular microarchitecture.

Microgravity also alters osteoblast-like cells *in vitro.* During the Biocosmos-10 space flight, we showed that the proliferation of ROS 17/2.8 osteosarcoma cells was similar to that of ground controls, but these cells exhibited shape changes; some cells were rounder and piled up, while others were retracted and presented long cytoplasmic extensions, and a third population remained spread out, with a shape similar to that of ground controls and in-flight 1*g* centrifuge controls [2]. In a following study, we quantified cell shape parameters in ROS 17/2.8 cells after parabolic flight, which provides 20-s periods of true microgravity. Flight cells exhibited cytoplasmic retraction leading to stellar shapes [3]. However, this result could not be attributed exclusively to microgravity, as the mechanical environment during parabolic flight switches from hypergravity (2*g*) to microgravity ($10^{-2}g$). In this present study, we examined ROS 17/2.8 sensitivity to 3-h parabolic flight conditions (two ESA parabolic flight programs). We also performed various control experiments: a 3-h continuous 2*g* centrifugation on the ground, as well as a microgravity simulation in a clinostat. The clinostat is widely used on the ground to simulate microgravity conditions [4, 12]. Its principle of action is based on Gz randomization. Adherent cells cultured in the clinostat are unable to sense the gravity vector because its direction of application is always varying with horizontal rotation of culture tubes.

Most studies have focused on mechanical signal transduction with a biochemical approach, but little is known about the organization of one of the mechanotransductors, which is the cell adhesion structure [5]. Previous studies have suggested that mechanical stimulation involves the cytoskeleton and is mediated via focal adhesion plaques [6, 7]. Focal adhesion plaques connect actin stress fibers and an array of intracellular linker proteins [α-actinin, talin, vinculin] [8] to a transmembrane integrin bound to extracellular adhesion proteins, thus linking the cytoskeleton to the extracel-

[1] To whom correspondence and reprint requests should be addressed at LBTO, Faculté de Médecine, 15, rue Ambroise PARE, F-42023 Saint-Etienne Cedex 2, France. Fax: (33-4) 77 57 55 72. E-mail: lbto@univ-st-etienne.fr.

0014-4827/97 $25.00

lular matrix [9]. Focal contact assembly involves different events that are not fully understood. According to Miyamoto *et al.* [10] vinculin is one of the last proteins to colocalize to the integrin cluster—only when integrins have been bound to the extracellular matrix.

Detailed analysis of cell morphology and cell adhesion required quantification of cell structures. For example, in a previous study, we concomitantly analyzed interference contrast reflection images and vinculin immunofluorescence in order to quantitatively evaluate focal adhesion patterns. We previously showed that these combined measurements can be used to assess the dynamics of adhesion parameters in fixed cells [11]. We also observed that, in ROS 17/2.8, focal adhesion plaque organization is cell cycle-dependent. In addition, when cells are exposed to Gz randomization, mitotic cells proved to be less responsive than quiescent cells in terms of interference reflection images and vinculin spots [12].

The first aim of this study was to evaluate shape and focal adhesion in cells submitted to 0–2*g* switches or to continuous 0 and 2*g* exposure and, in a second step, to evaluate these same parameters in nocodazole-arrested mitotic cells. We developed a specific automatic image analysis software using confocal scanning laser images. This program allowed quantification of morphological parameters obtained either by interference contrast reflection images or by vinculin staining images. Concomitant analysis of these two types of focal adhesion images allowed determination of overlapping or isolated fractions of focal adhesion areas. Factorial discriminant analysis was used to identify the most discriminant of all of these parameters.

MATERIALS AND METHODS

Cell culture. The cells used in this study were rat osteosarcoma cells (ROS 17/2.8), a well-defined mature osteoblastic phenotype. The culture medium was DMEM supplemented with 10% fetal calf serum, 2 m*M* L-glutamine, and a 1% penicillin–streptomycin solution. Since no gas exchange occurs in our culture device, medium was buffered with 3.7 mg/L of $NaHCO_3$ and 20 m*M* Hepes. Under these conditions, cell growth and alkaline phosphatase activity are similar to those under normal O_2/CO_2 culture conditions [2]. Cells were plated on glass coverslips at a density of 5×10^4 cells/cm^2 and cultured at 37°C for 36 h. During transportation, cells were cultured at 24°C in a portable incubator (Steel). The culture temperature was switched to 37°C 18 h before the experiments. After the 15th and 30th parabolae of parabolic flight, cells were washed with PBS and fixed with 4% paraformaldehyde. Some cells were treated with 0.5 μg/ml of Nocodazole for 18 h (overnight treatment) after temperature switching to 37°C and were possibly submitted to *g*-level variations. All cells are submitted to identical timing and temperature switch. However, transport and take-off vibrations could not be mimicked in centrifuged and rotated cells.

The "Plunger-box" culture system. The hardware used for the parabolic flight and hypergravity experiment consisted of eight manual "plunger boxes" (C. C. M., The Netherlands). This cell culture device has been developed for space flight missions using a Biobox incubator and is composed of one or two culture chambers containing different compartments, filled with medium, buffer, and fixative. The medium is forced to the culture chamber by releasing a spring-loaded plunger by sequential manual activations that allow medium and fixative buffer changes.

Parabolic flight. Flights were performed during the 21st ESA campaign. The 2.5-h flight consisted of two groups of 15 parabolae. Each parabola lasted 3 min and included 30 s at 2*g*, 25 s at 0*g*, and 30 s at 2*g*. Five minutes of 1*g* flight separated each group of three parabolae. At predefined times (before the first parabola, after the 15th and 30th parabolae), one of us (A.G.) manually activated the plunger box units to rinse and fix cells. Total flight duration was about 3 h.

Centrifugation. The 3-h centrifugation was carried out using a commercial centrifuge that regulates temperature (Beckman, GPR). We developed a fixation system for plunger boxes in buckets fixed on the rotor of the centrifuge. Plunger boxes remained in the horizontal position during rotation so that the *g* forces were exerted transversely to the coverslip inside the plunger box. Force application had the same direction as during flight *g* variations. The radial distance to the axis of rotation was 10 cm and the rotation speed was 120 rpm. The *g*-level applied *g* (2*g*) was calculated according to the formula $g = ((r \cdot \omega^2/go)^2 + 1)^{1/2}$, where $\omega = 2\pi$ rpm/60 (rpm means rotation per minute); r is the radius (m); and $go = 9.81\ m \cdot s^{-2}$.

Clinostat. The clinostat (C. C. M., The Netherlands) is composed of three horizontal rotating tubes (ϕ 5 mm) and their three identical static tubes for control experiments. Cells were seeded (5×10^4/cm^2) on 5-mm-wide glass coverslips inserted and blocked in tubes (two coverslips/tube). The clinostat was placed in an incubator regulating the temperature at 37°C. The incubator was placed on an anti-vibration table. Theoretical considerations [4] and personal experience [12] were taken into account in defining optimal experimental procedures, in particular the 50-rpm rotation speed. The duration of clinorotation experiments was similar to that of parabolic flight (3 h).

Groups. Nine groups of cells were defined: 1G, ground basal control, 1*g* centrifugation; 2G, 3 h of continuous 2*g* centrifugation; F0, fixed in flight before *g*-level variation, 0 parabola experienced; F15, fixed in flight, 15 parabolae experienced (1.5 h of intermittent mechanical stress); F30, fixed in flight, 30 parabolae experienced (3 h of intermittent mechanical stress); F0-Noc, nocodazole treatment fixed in flight before *g*-level variation, 0 parabola experienced; F15-Noc, nocodazole treatment fixed in flight, 15 parabolae experienced; Clino0, control of clinorotation, static culture, 0 rpm; Clino50, rotated cells, clinostat speed of 50 rpm for 3 h.

Flow cytometry. DNA-associated propidium iodide was analyzed by flow cytometry [13]. Briefly, cells were washed in PBS and permeabilized in 70% ethanol. Then, the pellets were incubated in ribonuclease A (Sigma, 5503) and stained with propidium iodide (Sigma, 4170). Flow cytometry analyses were performed using a FACStar Plus cell sorter (Becton–Dickinson).

Immunofluorescence staining (IF). Cells were washed in PBS and fixed and permeabilized with 4% paraformaldehyde for 30 min followed by 0.1% Triton X-100. Nonspecific binding was blocked by incubation at 37°C in PBS/10% fetal bovine serum. Vinculin primary antibody (diluted 1/100) and conjugated FITC (1/64) were purchased from Sigma, France. Antibody incubations were performed at 37°C for 45 min. Cells were washed extensively in PBS between antibody incubations and were mounted in PBS/20% glycerol before confocal scanning laser examination.

Image analysis. Cell shape was analyzed with a semiautomatic image analyzer (SAMBA-Alcatel) on 30 to 40 cells per condition. Quantification was performed on confocal scanning laser images of vinculin staining or interference reflection microscopic images (CIRM) and was based on thresholding of vinculin adhesion plaques

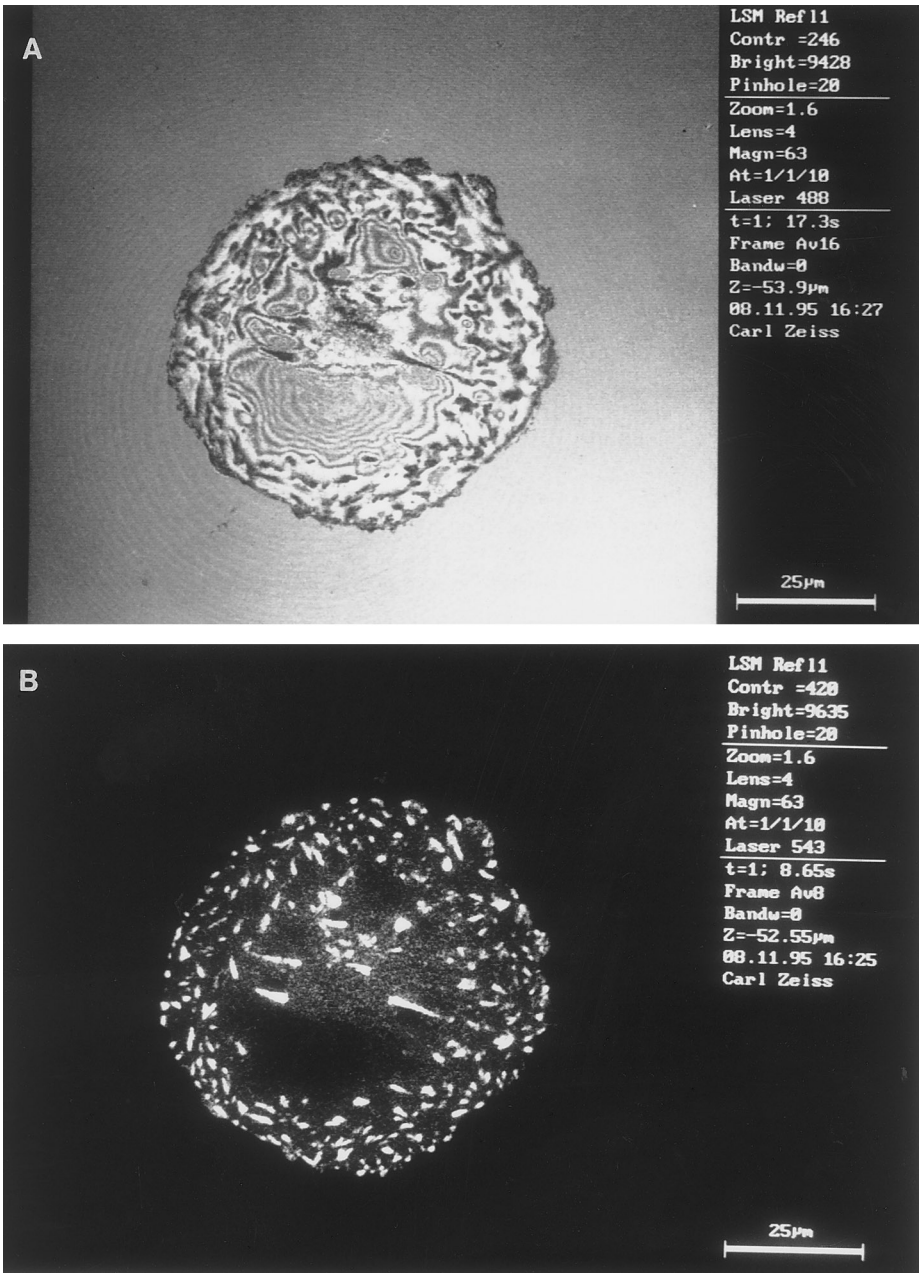

FIG. 1. Micrographs of focal contacts in ROS 17/2.8 cultured for 36 h in the plunger box culture system on glass coverslips. (A and B) Representative ROS 17/2.8 of 1G control group; (C and D) of the F0 flight group; and (E and F) of the F30 flight group. (B–D) Osteoblast stained for the presence of vinculin examined with a confocal laser scanning microscope at the focal contact plane (A, E, and F). Interference reflection contrast images (CIRM) of the cell shown respectively in (B–D). (A and B) Characteristics of confocal imaging are listed on images. Bars, 25 μm. (C–F) Saved images as they were treated for image analysis. Note the altered morphology of the cell in (D) compared to (B), with a decreased cell area and increased shape factor (perimeter irregularity). The comparison between representative cells from F0 (C) and F15 (E) indicated that the number of vinculin spots (*N*) was decreased. The delimited square area on the same cell (D and F) illustrates the fact that some IRM focal contact did not colocalize with vinculin. Bars, 20 μm.

and IRM cell/substratum contacts. We previously reported details of such an analysis [11]. Confocal images of 1*g* cells and representative cells of parabolic flight groups (F0 and F30) are shown in Fig. 1.

Statistical analysis. Multivariate analysis tools were used to discriminate groups and to assess the significance of measurements (or variables). In a first stage, all data were merged and the correlation matrix was calculated. Factorial discriminant analysis (FDA) is a multivariate statistical analysis designed to emphasize the difference between experimental groups, based on measurements of several parameters [14]. Results were expressed in the form of confusion

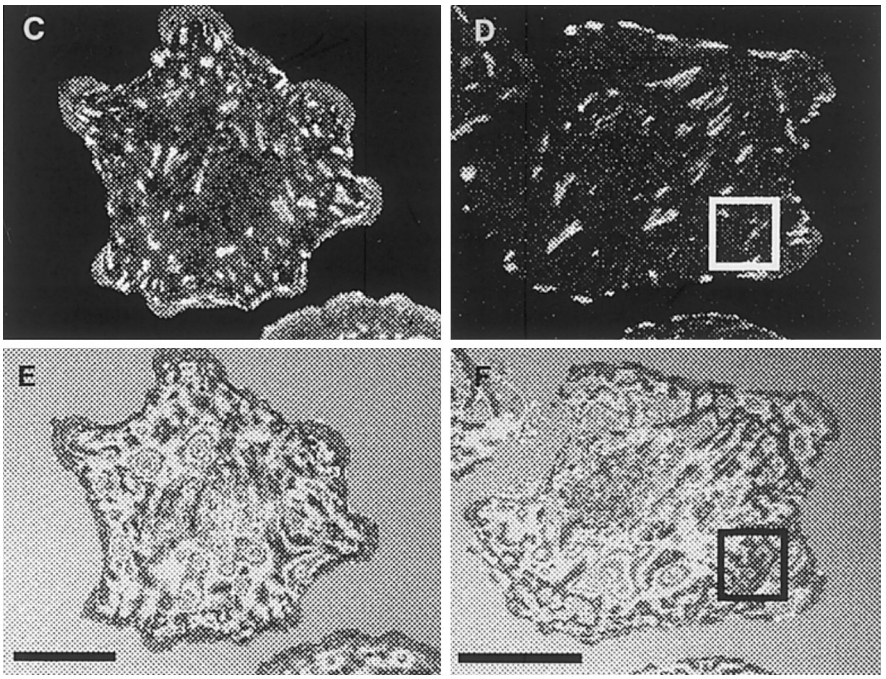

FIG. 1—*Continued*

matrices; the robustness of classification was ensured by using a "jackknife" procedure: the assignment of a single cell was tested against the a posteriori probabilities involving all other cells except this cell [14]. Using the most discriminant parameters, derived from stepwise analysis, a Mann–Whitney test was used to compare the various groups.

RESULTS

Selected Parameters

Image analysis can be used to quantify many morphological and topographic parameters. Morphological parameters included cell area, shape factor, and cell ratio. Focal adhesion parameters (Fig. 1) were determined either by IRM, expressed as the percentage of cell area in close contact with the substratum, or by IF, expressed as the relative area of vinculin per cell and the number, density, mean area, length, distribution—average distance from the edge—and alignment—angular span—of vinculin containing plaques or spots. After sorting by discriminant analysis, we adopted the most discriminant parameters: CA, cell area; SF, cell shape factor (perimeter/πr^2); IRM, physical contact area from reflection contrast images normalized by CA; IF, focal contact vinculin positive area, from immunofluorescence images normalized by CA; *N*, number of vinculin spots per cell; and IFi, isolated

TABLE 1

Stepwise Discriminant Analysis

Step	Parameters	Discriminant power	% Classification error
1	**IRM** (Relative focal contact area)	**76.4**	**61**
2	***N*** (Number of vinculin spots)	**32.5**	**40**
3	IFi (Isolated vinculin staining area)	18.7	33.7
4	SF (Shape factor)	5.6	26.7
5	CA (Cell area)	4	22

Note. Bold: parameters further used for group to group comparisons. Note that the first two steps IRM and *N* are obtained from independent images and both related to focal adhesion parameters. Morphological parameters such as shape factor (SF) and cell area (CA) are only reported in the 4th and 5th steps.

TABLE 2

Confusion Matrix after Step 5 of Stepwise Discriminant Analysis, in Which Rows Correspond to the Group of Origin and Columns Correspond to a Posteriori Group Assignment of Cells

Groups	F0	F15	F30	1G	2G	Clino0	Clino50
F0 (*n*: 34)	**28**	1	3	0	0	2	1
F15 (*n*: 30)	1	**23**	6	0	0	0	0
F30 (*n*: 32)	3	4	**25**	0	0	0	0
1G (*n*: 30)	0	0	0	**25**	0	1	4
2G (*n*: 28)	0	0	0	3	**12**	1	2
Clino0 (*n*: 32)	2	1	0	1	2	**23**	3
Clino50 (*n*: 45)	2	0	0	2	3	2	**36**

Note. Bold: number of cells correctly assigned to their group. For example, in the first line 28 cells/34 were correctly assigned to F0, 1 was assigned to F15, and 3 were assigned to F30.

fraction of vinculin staining, IF non-overlapping IRM physical contact zones.

Comparison between Intermittent and Continuous Gz Variations

Selection of the two most discriminant parameters (FDA). The first analysis was performed on all groups except for the groups of nocodazole-treated cells. The stepwise analysis and the confusion matrix are reported in Tables 1 and 2, respectively. Table 1 shows the first five steps of the descriptive analysis. IRM and *N* were the most discriminant parameters and were consequently submitted to comparative analysis. Table 2 shows the retrospective classification of the cells. A very good classification was observed between cells from flight groups (F0, F15, and F30) and those from centrifuged and rotated groups, although a certain confusion was observed between F15 and F30 and between 1G and Clino0. This analysis was therefore able to select the main variables that discriminate the various groups: physical adhesion of the cells to their substratum (IRM) and the number of vinculin spots (*N*).

Effect of Gz variations on these two parameters: Physical Contact Area (IRM) (Fig. 2). The physical contact areas occupied 40% of the cell area in group 1G. In the control groups (1G, F0, and Clino0), differences were observed between F0 and 1G (−20%), suggesting that transport and take-off vibrations decreased IRM. Both F15 and F30 showed lower values than F0: −20 and −10%, respectively. The F30 value was significantly higher than the F15 value, suggesting cell adhesion adaptation to the parabolic flight conditions. Continuous 2*g* exposure or clinorotation did not change physical contact areas compared to their respective controls.

Number of vinculin spots per cell (N) (Fig. 3). Sim-

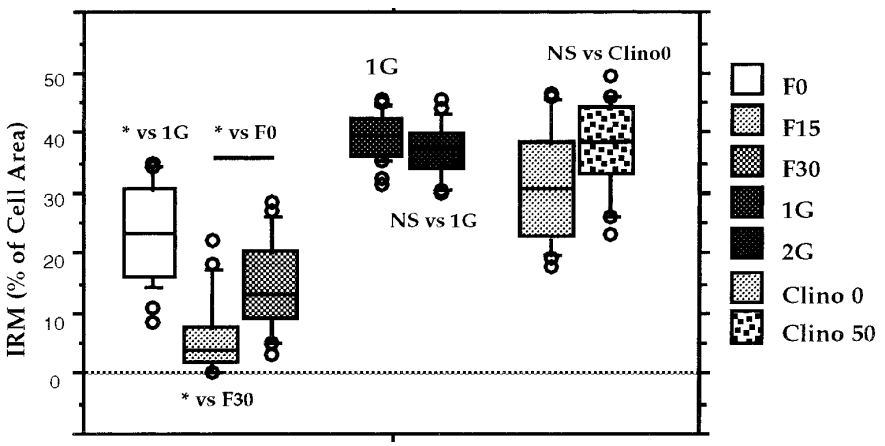

FIG. 2. Comparison of relative focal contact area (IRM) between groups. Box plots and whiskers of IRM (upper and lower lines indicate the 10th and 90th percentiles, boxes the 25th and 75th percentiles, and the line in the box the median). IRM is expressed in percentage of cell area. We showed that after 15 parabolae (F15), IRM is greatly reduced compared to F0 and F30, suggesting a biphasic adaptation of focal adhesion to the flight. Comparison of Clino50 and 2G with their respective control groups (Clino0 and 1G) did not show any differences.

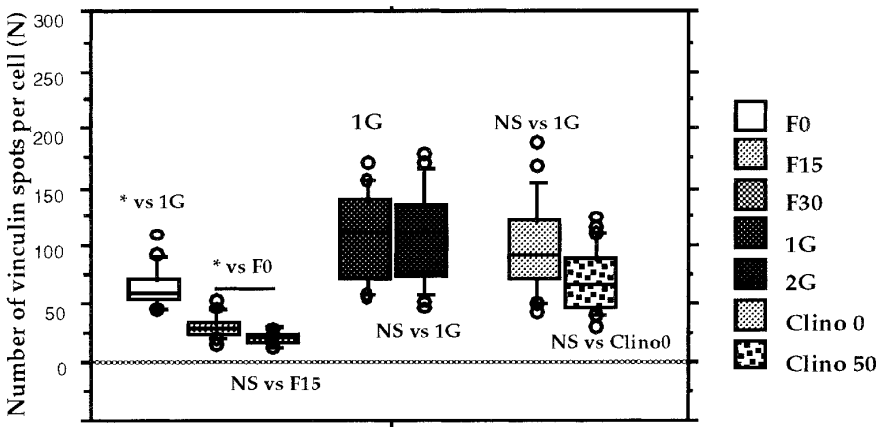

FIG. 3. Box and whiskers of number of vinculin spots per cell (*N*). The number of vinculin spots decreased significantly during the first part of the flight (15 parabolae) and remained low at F30 compared to F0. A significant difference was found between F0 and 1G, indicating that transport and take-off vibrations decreased the vinculin spot number before Gz variations. Comparison of Clino50 and 2G with their respective control groups (Clino0 and 1G) did not show any difference. Note the wide dispersion of values in those groups.

ilarly to IRM, F0 showed a lower vinculin spot number than in 1G and Clino0 control groups. In contrast with IRM, the number of vinculin spots decreased continuously during flight, with F15 decreased by 50% and F30 decreased by 75% compared to F0. No alteration of the number of vinculin spots was observed in the centrifuged and clinostated groups.

In summary, the variations between 0 and 2 Gz in-

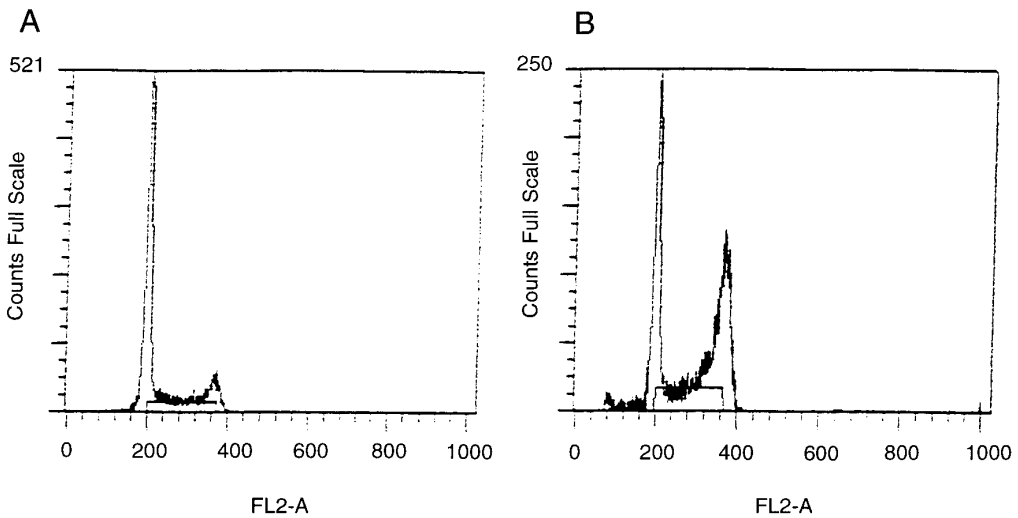

C

Phases	Non-synchronous	Nocodazole treatment
G1	62.5 %	29 %
S	26 %	28 %
G2/M	**11.5**	**43 %**

FIG. 4. Cytometric analysis performed on ROS 17/2.8 stained with propidium iodide (PI) (A) Nonsynchronized cells; (B) cells treated with 0.5 μg/ml of nocodazole for 18 h. (C) Cell cycle statistics, with bold percentage of mitotic cells in control and nocodazole-treated cells.

TABLE 3

Stepwise Discriminant Analysis

Step	Parameters	Discriminant power	% Classification error
1	**CA** (Cell area)	**82.2**	**52.2**
2	**IF** (Relative vinculin area)	**38**	**36**
3	IRM (Relative focal contact area)	13	25
4	IFi (Isolated vinculin staining area)	6	24.8
5	SF (Shape factor)	4	21.7

Note. Bold: parameters further used for group to group comparisons. Cell area (CA) had the highest discriminant power (82.2%). Providing independent information, relative vinculin area, and relative focal contact area were also normalized by this morphological parameter.

duced a continuous reduction of the number of vinculin spots, while the physical contact area decreased after 15 parabolae and then rose after the 30th parabola. In contrast, we did not detect any difference between the groups submitted to hypergravity or continuous simulated microgravity. The effects of nocodazole will therefore be studied exclusively on cells subjected to parabolic flight conditions.

Effect of Nocodazole Treatment on Flight Cells

Synchronization by nocodazole (Fig. 4). Flow cytometry of nocodazole-treated cells showed that a higher proportion of ROS 17/2.8 cells were in G2/M phase (43%) compared to asynchronous cells (11.5%). Consequently, the G1 cell fraction was markedly decreased by treatment, as shown in cell cycle statistics.

Factorial discriminant analysis. Parameters in F0, F15, F30, and the nocodazole-treated groups F0-Noc and F15-Noc were submitted to discriminant analysis. The stepwise analysis and the confusion matrix are shown in Tables 3 and 4, respectively. Table 4 shows that some confusion in classification persisted for nocodazole-treated cells (10 cells of F0-Noc were assigned to F15-Noc). The main parameters selected in this case were CA, IF, IRM, IFi, and SF. As in the previous study, the first two parameters were compared between groups.

TABLE 4

Confusion Matrix after Step 5 of Stepwise Discriminant Analysis, in Which Rows Correspond to the Group of Origin and Columns Correspond to a Posteriori Group Assignment of Cells

Groups	F0	F15	F30	F0-Noc	F15-Noc
F0 (*n*: 34)	**29**	0	5	0	0
F15 (*n*: 30)	1	**18**	10	0	0
F30 (*n*: 32)	2	2	**28**	0	0
F0-Noc (*n*: 31)	0	0	1	**20**	10
F15-Noc (*n*: 34)	0	0	5	7	**22**

Note. Bold: number of cells correctly assigned to their group. For example, in the first line 29 cells/34 were correctly assigned to F0 and 5 were assigned to F30.

Effect of Gz variations on cell area (Fig. 5). The cell area was decreased significantly after the 15th and the 30th parabolae (−30% for F15 and −40% for F30) compared to F0. Treatment with nocodazole induced very marked cell retraction in controls (−50% F0-Noc), which was not accentuated during flight (−50% F15-Noc). Nocodazole, which induced maximal reduction of cell area, inhibited any additional retraction during flight.

Effect of Gz variations on vinculin staining area (Fig. 6). The vinculin staining area decreased continuously during flight (−10%, F15 vs F0, and −20%, F30 vs F0). This result can be explained by the previously observed reduction of *N* (Fig. 2), especially as the mean area of the spots was never modified (data not shown). F0 was significantly lower than F0-Noc, which shows that treatment with nocodazole inhibits the relative reduction of IF at the beginning of flight (take-off and 45 min of normal flight). No change in F15-Noc vs F0-Noc was observed after 15 parabolae. However, a marked scatter of the values was observed in the Noc groups, probably related to the different responses of the 40% of cells in G2/M compared to the remaining 60% (Fig. 4). The vinculin staining area is a very sensitive parameter to experimental conditions. Nocodazole, which preserves IF, therefore largely inhibits the effect of flight, visible from take-off.

DISCUSSION

It is well known that bone tissue adapted its mass and microarchitecture to mechanical environment. Altered osteoblast activity and recruitment were significant findings in models of skeletal loading/unloading leading to the hypothesis that osteoblast lineage cells are specialized for receiving and transmitting mechani-

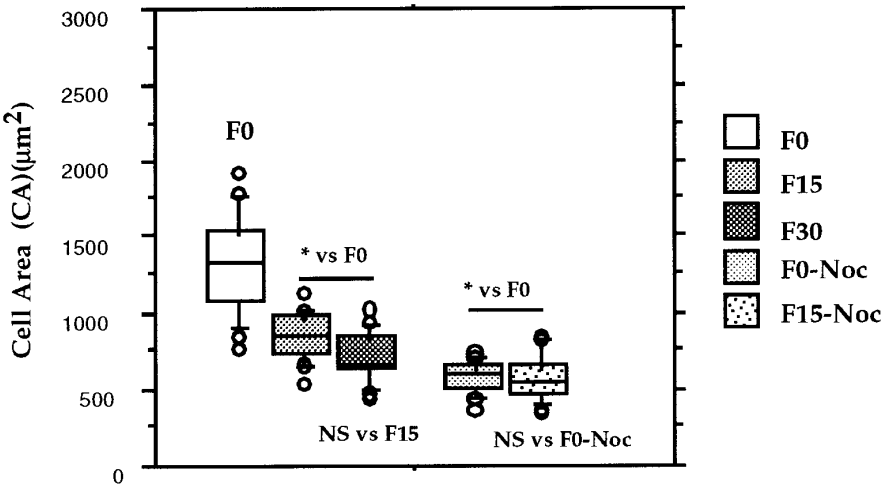

FIG. 5. Box plot and whiskers of cell area (CA). Cell area of nocodazole-treated groups was dramatically reduced compared to F0 untreated group. Gz variations led to a significant cell retraction after 15 parabolae and remained stable after 30 parabolae, given the major cell retraction measured in F0-Noc. The flight-induced decrease of the cell area seen in the F15 group was not observed in the F15-Noc group.

cal stimuli. To begin to investigate, at the cellular level, how gravitational variations are transmitted to the osteoblastic cells, we focused on adhesion structures, in particular focal adhesions, which appeared to be good candidates as "mechanoreceptor and transducer" because they physically link the extracellular matrix to the cytoskeleton.

Parabolic flights are usually models of short periods of true microgravity [14, 15]. However, as it is difficult to identify the specific effects of 2 and 0*g* (2*g* of acceleration of the plane occurs on either side of microgravity periods during each parabola), we have interpreted the results of parabolic flight as the result of intermittent gravitational stress. In order to more clearly understand the effects of either microgravity or hypergravity, we submitted cells to an exposure equivalent to the duration of flight for each level of *g:* 0, 1, and 2*g*.

Schmitt *et al.* [15] showed that PKC-dependent pathways, whose sensitivity to microgravity has been previously demonstrated by several authors [16, 17], were

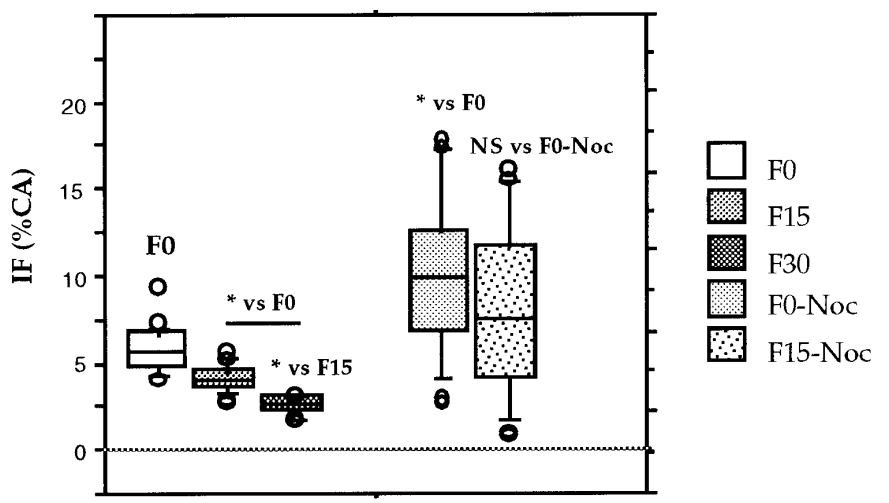

FIG. 6. Box and whiskers of relative vinculin area (IF) show the constant decrease of vinculin area during the flight. No difference was found between F0-Noc and F15-Noc groups, suggesting that nocodazole treatment before Gz variations prevented the flight-induced decrease observed in nontreated cells. Note the wide distribution of IF in nocodazole-synchronized cells, suggesting an incomplete synchronization by nocodazole before the flight (40%).

not affected by short periods of microgravity during parabolic flight. However, the apparent discrepancy between Schmitt *et al.* [15] and Rijken *et al.* [16] could be explained either by hypergravity per se or by 0–2*g* switches that may affect the observed cellular response during 0*g* periods. Cellular responses whose activation and return to normal occur within 20 s can be studied at 2 or 0*g* (phosphorylation, protein translocation, secondary messengers such as calcium, IP3, cAMP). For example, Jones [18] demonstrated an increase in intracellular calcium in osteoblasts during periods of microgravity. Cellular responses during flight can also be monitored, as reported by Armstrong *et al.* [19], who showed that the cellular adhesion of macrophages, evaluated by impedance measurements, increased during microgravity periods and returned to basal level during hypergravity periods. However, in this case, cellular responses might also be associated not only with the level of *g* but also with the variations of *g*.

In our study, the time course imposed by parabolic flights was respected in all groups. However, the vibrations related to transport could not be reproduced for the 1G, 2G, and clinorotated groups. The reduction of the cell area, number, and relative area of vinculin staining as well as the IRM between F0 and 1G cells therefore demonstrated that the associated transport and vibration conditions had already sensitized ROS 17/2.8 cells. The appropriate control group, which allows demonstration of the specific effect of 0–2*g* variations is the F0 group, for which cells are fixed in flight just before Gz variations.

In our study, ROS 17/2.8 cells globally decreased all of their adhesion parameters, both IRM and IF, during flight. In contrast, these parameters remained unchanged during continuous exposure regardless of the level of *g* applied for a period of 3 h. However, for longer exposures to microgravity [2] or clinostat [11], the morphology and the focal adhesion of ROS 17/2.8 cells were modified. Moreover, cytoskeleton reorganization was reported by Hughes-Fulford and Lewis [20], who demonstrated an alteration of actin assembly in another osteoblastic cell line, MC3T3-E1, submitted to a 4-day space flight. In our study, the number of vinculin contacts regularly decreased during parabolic flight, while IRM decreased after the 15th parabola, before rising again after the 30th parabola, without, however, reaching the F0 control level. This suggests that adaptation of the cell is dynamic and that, after a 3-h flight, new non-vinculin-dependent physical contacts have been developed. These new contacts may be either immature integrin-dependent focal contacts [21] or other adhesive molecules not including integrins (immunoglobulin-like proteins, selectins, CD 44, and OSF-1 and -2, all described in osteoblasts [22]).

We therefore observed modifications of cellular responses to intermittent variations of Gz and not to constant levels. These results are in line with those of *in vivo* and *ex vivo* studies showing that osteogenic cellular responses leading to increased bone mass [23] appear to be activated preferentially by intermittent rather than continuous strains [24].

However, *in vitro* results are less concordant, as some authors have shown an increased proliferation of MC3T3-E1 cells via PGE2-mediated mechanisms under continuous hypergravity [25], while others have demonstrated that intermittent forces produce an increase in DNA synthesis when compared to static or continuous forces [26]. Another important determinant in osteoblastic response is the magnitude of the applied stress. Burger and Veldhuijzen [27] pointed out that cells increased their proliferation rate when submitted to high stress, whereas they increased their differentiation under low stress levels. Overall, these studies do not indicate whether modifications of cellular adhesion are involved. The absence of modification of our parameters at 2*g* can be interpreted by the constancy of the applied stress, but also by the low level of *g*, as Nakajima has shown that proliferation of MC3T3-E1 cells is increased from the nonphysiological level of 20*g* [23].

In a previous study, we showed that focal contacts of mitotic cells are not modified by variations of mechanical constraint, in contrast with interphase cells [4]. In this study, we pretreated parabolic flight cells with nocodazole, which inhibits microtubule polymerization and consequently synchronizes cells in phase G2/M [28, 29]. This pretreatment inhibits the reduction of the number of vinculin spots per cell as well as the reduction of physical adhesion to the substratum (IRM) observed in nontreated cells. This treatment therefore shows that the adaptive response of ROS cells at least depends on microtubule function and that their integrity must be preserved before focal contact disassembly and assembly can occur. It therefore appears obvious that any structural modification induces modification of this response.

Although the contributions of the actin bundles to focal adhesions has been extensively studied, less is known about possible interactions with microtubules. Recently, Troyer *et al.* [30] showed that, in mesengial cells, the organization of microtubules appeared intimately related to focal adhesion via phosphorylation of p125FAK. Disruption of microtubule assembly with colchicine reduced adhesion in ligament fibroblasts [31]. This result was in line with that of the present study. However, Bershadsky *et al.* [32] showed that disruption of microtubules by nocodazole or vinblastine induces rapid assembly of focal adhesions and microfilament stress fibers in serum-starved Swiss 3T3 cells. Taken together, these results showed that the microtubule system was a determinant cytoskeletal element

in focal contact organization, although the results appeared not yet concordant.

In conclusion, this study showed that the interpretation of results obtained after parabolic flights requires appropriate control experiments such as hypergravity and simulated microgravity (as there is no other way of obtaining 3 h of continuous real 0*g*). ROS 17/2.8 cells were shown to adapt their shape and focal adhesions when submitted to small switches of Gz, whereas these structures remained stable after 3 h of constant and low-level Gz. We also showed that this adaptation was abolished by nocodazole treatment, suggesting that reorganization of adhesion plaques depends, at least partially, on microtubule function. Thus, as a first step, we described responses of osteoblastic cells to *g* variations in terms of focal contact pattern, cytoskeleton, and cell cycle. These early responses will induce changes in cell differentiation and function, with the major consequences we see at the tissue level. These events remain to be investigated.

REFERENCES

1. Rodan, G. A. (1991) *J. Bone Miner. Res.* **6,** 527–530.
2. Guignandon, A., Genty, C., Lafage, M. H., Vico, L., Palle, S., and Alexandre, C. (1997) *Bone* **20,** 109–116.
3. Guignandon, A., Vico, L., Alexandre, C., and Lafage-Proust, M. H. (1995) *Cell Struct. Funct.* **20,** 369–375.
4. Block, I., and Briegleb, W. (1986) *Eur. J. Cell Biol.* **41,** 44–50.
5. Ingber, D. (1991) *Curr. Opin. Cell Biol.* **3,** 841–848.
6. Clark, E. A., and Brugge, J. S. (1995) *Science* **268,** 233–239.
7. Wang, N., Butler, J. P., and Ingber, D. E. (1993) *Science* **260,** 1124–1127.
8. Aarden, E., Nijweide, P., van der Plas, A., Alblas, M., Mackie, E., Horton, M., and Helfrich, M. (1996) *Bone* **18,** 305–313.
9. Ingber, D., and Folkman, J. (1989) *J. Cell Biol.* **109,** 317–330.
10. Miyamoto, S., Teramoto, H., Coso, O., Gutking, J., Burbelo, P., Akiyama, S., and Yamada, K. (1995) *J. Cell Biol.* **131,** 791–805.
11. Usson, Y., Guignandon, A., Laroche, N., Lafage-Proust, M. H., and Vico, L. (1996) Cytometry. [In press]
12. Guignandon, A., Usson, Y., Laroche, N., Vico, L., Alexandre, C., and Lafage-Proust, M. H. [Submitted for publication]
13. Sabido, O., Alamartine, E., Barthelemy, J. C., and Berthoux, F. (1991) *Transplantation* **52,** 467–470.
14. Mainly, B. (1986) *in* Multivariate Statistical Analysis: A Primer, pp. 86–99, Chapman & Hall, London.
15. Schmitt, D. A., Ohlmann, P., Gachet, C., and Cazenave, J. P. (1993) *J. Cell Sci.* **104,** 805–810.
16. Rijken, P., de Groot, R., Briegleb, W., Kruijer, W., Verkleij, J., Boonstra, J., and de Laat, S. (1991) *Aviat. Space Environ. Med.* **62,** 32–36.
17. Woods, K. M., and Chapes, S. K. (1994) *Exp. Cell Res.* **211,** 171–174.
18. Jones, D. B., Brockmann, E., Sasse, L., Van der Sloten, J., Goodship, A., Leivseth, G., and Tenbosch, J. (1996) *Low G.* **7,** 14–17.
19. Armstrong, J. W., Gerren, R. A., and Chapes, S. K. (1995) *Exp. Cell Res.* **216,** 160–198.
20. Hughes-Fulford, M., and Lewis, M. L. (1996) *Exp. Cell Res.* **224,** 103–109.
21. Miyamoto, S., Teramoto, H., Coso, O., Gutking, J., Burbelo, P., Akiyama, S., and Yamada, K. (1995) *J. Cell Biol.* **131,** 791–805.
22. Gieffers, C., Engelhardt, W., Brenzel, G., Matsuichi, T., and Frey, J. (1993) *Eur. J. Cell Biol.* **62**(2), 352–361.
23. Bourrin, S., Palle, S., Pupier, R., Vico, L., and Alexandre, C. (1995) *J. Bone Miner. Res.* **10,** 1745–1752.
24. Lanyon, L. E. (1987) *J. Biomech.* **20,** 1083–1093.
25. Nakajima, T. (1991) *Kokubyo Gakkai-Zasshi* **58,** 529–544.
26. Sandy, J. R. (1993) *Br. J. Orthod.* **20,** 1–11.
27. Burger, E. H., and Veldhuijzen, J. P. (1993). *In* "Bone Growth" (B. K. Hall, Ed.) pp. 37–56, CRC Press, Boca Raton, FL.
28. Masson, D., and Kreiss, T. E. (1995) *J. Cell Biol.* **131,** 1015–1024.
29. Wang, Y., and Burke, D. J. (1995) *Mol. Cell Biol.* **15,** 6838–6844.
30. Troyer, D. A., Bouton, A., Bedolla, R., and Padilla, R. (1996) *J. Am. Soc. Nephrol.* **7,** 415–423.
31. Sung, K. L., Yang, I., Whittemore, D. E., Shi, Y., Jin, G., Hsieh, A. H., Akeson, W. H., and Sung, L. A. (1996) *Proc. Natl. Sci. USA* **93,** 9182–9187.
32. Bershadsky, A., Chausovsky, A., Becker, E., Lyubimova, A., and Geiger, B. (1996) *Curr. Biol.* **6,** 1279–1289.

Received February 12, 1997
Revised version received June 26, 1997